Tin-oxide overlayer formation by oxidation of Pt–Sn(111) surface alloys

Cite as: Journal of Vacuum Science & Technology A **19**, 1953 (2001); https://doi.org/10.1116/1.1345902
Submitted: 14 September 2000 . Accepted: 04 December 2000 . Published Online: 13 July 2001

Matthias Batzill, David E. Beck, Dmitri Jerdev, and Bruce E. Koel

Tin-oxide overlayer formation by oxidation of Pt–Sn(111) surface alloys

Matthias Batzill, David E. Beck, Dmitri Jerdev, and Bruce E. Koel[a)]
Department of Chemistry, University of Southern California, Los Angeles, California 90089-0482

(Received 14 September 2000; accepted 4 December 2000)

Ordered (2×2) and ($\sqrt{3}\times\sqrt{3}$)*R*30° Pt–Sn(111) surface alloys were oxidized by NO_2 exposure at 400 K under ultrahigh vacuum conditions. The evolution of the surface morphology with annealing temperature was characterized by using low energy electron diffraction (LEED), scanning tunneling microscopy, Auger electron spectroscopy, and x-ray photoelectron spectroscopy. Both oxidized surface alloys form a SnO_x overlayer that wets the substrate. However, the SnO_x film does not completely cover the surface for the oxidized (2×2) surface alloy. For the oxidized ($\sqrt{3}\times\sqrt{3}$)*R*30° surface alloy, an ordered (4×4) LEED pattern is formed upon flash annealing above 900 K. The formation of this ordered SnO_x adlayer coincides with Sn segregation from the bulk to the interface region. A model for the (4×4) structure is discussed. The SnO_x overlayer formed by oxidation of the (2×2) surface alloy is significantly less thermally stable than the oxidized ($\sqrt{3}\times\sqrt{3}$)*R*30° surface alloy. Exothermic alloying of Sn with Pt may facilitate the decomposition of the oxide overlayers. Differences in the amount of subsurface tin and its segregation to the surface is proposed to explain the thermal stabilities of the oxide layers. The incompleteness of the SnO_x overlayer and less subsurface tin for the oxidized (2×2) surface alloy is proposed to explain its significant lower thermal stability. © *2001 American Vacuum Society.* [DOI: 10.1116/1.1345902]

I. INTRODUCTION

Oxidation studies of Pt–Sn surface alloys are motivated by the important technological role of this system. Tin–platinum bimetallic catalysts are important for hydrocarbon reforming.[1–4] Sn addition to Pt supported on alumina increases catalyst lifetimes through improved resistance against coking. Also, Pt supported on tin-oxide catalysts is used for CO oxidation.[5] Furthermore, SnO_2 is widely used in gas sensors for toxic gases like CO, NO_2, O_3, etc., and Pt is sometimes used as a promoter in these gas-sensing devices. From these and other various applications of Sn/Pt alloys and Pt particles on SnO_2 supports, it is apparent that the SnO_x/Pt interface plays an important role in the reactivity of these materials and deserves further study.

Studies of the oxidation and reduction of bulk Pt–Sn alloys and Pt particles supported on SnO_2 have been performed by Auger electron spectroscopy (AES),[6–11] angle-resolved auger electron spectroscopy (ARES),[12,13] x-ray photoelectron spectroscopy (XPS),[11,14] and ion scattering spectroscopy (ISS).[8–11] For Pt crystallites supported on SnO_2, Sn–O–Pt bonding was identified using XPS.[15,16] Furthermore, reduction of such samples was reported to form Pt–Sn alloys.[3,17–19] Oxidation of bulk Pt–Sn alloys at low temperatures ($T<500$ K) apparently forms a ''quasimetallic'' state of Sn (Sn–O–Pt bonding), while oxidation at higher temperatures results in an ''oxidic'' Sn state (SnO_x). Sn segregation to the surface at elevated temperatures resulted in the growth of multilayer oxide films for bulk alloys. We have recently focused on oxidation studies of Sn/Pt *surface* alloys with the advantage that the Sn available for oxidation is limited and thus ambiguities in the Sn-oxide composition and film thickness are reduced. However, even for these surface alloys, some small amount of subsurface tin is always present[20] and may segregate to the surface.

Evaporation of Sn onto a Pt(111) single crystal forms two stable surface alloys, the (2×2) and the ($\sqrt{3}\times\sqrt{3}$)*R*30° surface structure, depending on the initial Sn coverage.[21–23] Oxidation of these surface alloys at 300 K was previously studied under ultrahigh vacuum (UHV) conditions using ozone.[24,25] The O_2 temperature programmed desorption (TPD) curves from these two surfaces were distinctively different. After extensive oxidation, both TPD traces showed a large oxygen desorption peak at ~800 K that can be associated with decomposition of PtO_x. However, oxygen desorption from SnO_x decomposition occurred in a clearly separated, second desorption peak at 1050 K for the ($\sqrt{3}\times\sqrt{3}$)*R*30° alloy and in a small shoulder extending from the first oxygen peak at 800 K up to about 1000 K for the (2×2) alloy with no peak at 1050 K. It was speculated that this broad feature in the TPD curve was somehow due to islands of the SnO_x film. Island-size dependent SnO_x decomposition temperatures and/or rapid island-edge decomposition kinetics were proposed to explain the wide temperature range of oxygen evolution from this surface.

In this article, we extend previous studies discussed above with a more detailed structural characterization of the Sn-oxide adlayer formed by oxidation of two Pt–Sn(111) surface alloys. This work has allowed us to shed new light on the peculiar differences in the O_2 TPD curves observed between the oxidized (2×2) and ($\sqrt{3}\times\sqrt{3}$)*R*30° Pt–Sn(111) surface alloys.

Studies of other ultrathin oxide films on Pt(111) are related to our studies of the oxidation of Pt–Sn alloys and the formation of SnO_x layers on Pt(111). The oxidation of Ce,[26] Al,[27] Cr,[28] and Fe (Refs. 29 and 30) on Pt(111) were reported recently. For all these systems the formation of an ordered

[a)]Electronic mail: koel@chem1.usc.edu

overlayer was observed following annealing of the sample. The formation of tin oxide layers on Au(111) (Ref. 31) and on Pd(111) (Ref. 32) was also studied previously. Oxidizing a tin overlayer on gold and subsequent annealing were found to result in a disordered oxide layer, while oxidation at elevated temperatures (500–800 K) formed an ordered SnO_2 overlayer. However, at least half of the adlayer tin diffused into the gold crystal under these conditions. The oxidation of a Sn overlayer on Pd(111) is of particular relevance for this article, because the Pd/Sn system behaves much like Pt/Sn with respect to the formation of stable surface alloys.[33] It was suggested that submonolayer amounts of Sn oxidized to a stoichiometry of SnO on Pd(111). Furthermore, the thermal stability of these oxide layers was markedly less than for bulk Sn oxide samples and it was concluded that exothermic Pd/Sn alloying promotes the redox chemistry of tin oxide films.

II. EXPERIMENTAL METHODS

Experiments were performed in an UHV chamber, equipped with a cylindrical mirror analyzer (CMA) for AES, rear view low energy electron diffraction (LEED) optics, a quadrupole mass spectrometer for residual gas analysis and TPD, a homebuilt single-piezo-tube scanning tunneling microscope (STM), an ion gun for sample cleaning, a resistively heated Sn-evaporation source, precision-leak valves for gas dosing, including one directed-beam gas doser for NO_2 exposure. For AES, the electron gun and energy analyzer were positioned normal to the sample surface. The sample was heated by electron beam heating from the backside of the crystal. The sample temperature was measured by a Chromel/Alumel thermocouple spotwelded directly to the side of the crystal.

The Pt(111) single crystal was cleaned by standard procedures, consisting of cycles of 500 eV Ar^+ ion sputtering and annealing to 1200 K, annealing at 1000 K in 2×10^{-7} Torr O_2 to remove carbon, and finally, annealing to 1200 K in vacuum. The cleanliness of the sample was monitored by AES and the procedure was repeated until no contamination of the surface could be detected. The Sn deposition rate was calibrated by means of AES ''uptake'' plots of the AES signals as a function of Sn deposition time. From this we estimated a deposition rate of 0.01 monolayer (ML)/s, which was kept constant for all experiments. After every tin deposition we confirmed the tin coverage by measuring the Sn (430 eV) to Pt (237 eV) peak-to-peak ratios in AES. Sn/Pt surface alloys were formed by following the procedures outlined by Paffett and Windham.[21] Either ~0.4 or ~1.0 ML of Sn was deposited at ~350 K to form the (2×2) or $(\sqrt{3}\times\sqrt{3})R30°$ surface alloy, respectively, after subsequent annealing of the sample to 1000 K for 10 s.

In order to oxidize the alloy surfaces, NO_2 was dosed onto the sample at 400 K for 40 s at a background pressure of 4×10^{-8} Torr. NO_2 is known to be an extremely effective oxidant for metals, establishing very high ''effective'' O_2 pressures.[34–37] Under the conditions chosen no nitrogen contamination of the sample was detected by AES. After oxidation, the sample was flash annealed to several target temperatures and the resulting surfaces were characterized.

XPS studies of these surfaces were performed in another UHV chamber using another Pt(111) single crystal. Sample preparation and cleaning were identical to that described above. The chamber was equipped with a LEED optics, Mg $K\alpha$ (1253.6 eV) x-ray source and spherical capacitor electron energy analyzer (SCA). The x-ray incidence angle and the electron exit (SCA) angle were both 45° with respect to the sample normal. XPS spectra were recorded with the SCA at a pass energy of 29.35 eV. A Shirley background was subtracted from the measured spectra and peaks were analyzed using a least-square fitting procedure. LEED was used to characterize the oxidized alloy surfaces in this chamber, too.

III. RESULTS

Reduction of the oxidized (2×2) and $(\sqrt{3}\times\sqrt{3})R30°$ Pt–Sn(111) surface alloys with annealing temperature was characterized by AES and XPS. Information on the surface structure during reduction was obtained by using LEED and STM.

A. AES

AES spectra obtained during annealing for both oxidized surface alloys are shown in Fig. 1. A plot of the O (510 eV)/Sn (430 eV) peak-to-peak ratios [Fig. 1(c)] shows essentially the same reduction behavior as was reported previously following oxidation using ozone,[24] although oxidation with NO_2 produces a lower initial oxygen concentration compared to O_3. Most of the oxygen desorbs from the surface upon annealing to 820 K and is associated with reduction of PtO_x. For the (2×2) alloy, the O (510 eV) signal rapidly decreases with higher annealing temperatures and all oxygen is gone at 950 K. However, the O (510 eV) signal for the oxidized $(\sqrt{3}\times\sqrt{3})R30°$ alloy does not change significantly between 840 and 1020 K. At 1020 K, the SnO_x film starts to decompose and no oxygen remains at the surface at 1060 K.

B. XPS

XPS intensities provided results consistent with the AES data, but also gave complementary information on the chemical (oxidation) states of Pt and Sn. NO_2 dosing caused a small shift of the Pt($4f$) peak (+0.2 eV), indicating that Pt is partly oxidized at the surface. The peak position returns to that of clean Pt after annealing the oxidized alloy to 840 K. This observation supports the interpretation that PtO_x decomposition at this temperature evolves O_2 and decreases the oxygen peak in the AES spectra (Fig. 1). The changes in the Sn($3d$) peaks with annealing temperature are more clearly resolved because Sn is only present at the surface. However, assignment of chemical shifts in XPS to oxidation states of Sn has been reported to be difficult.[32,38] For the ultrathin SnO_x islands and films formed in this study, additional problems could arise from the influence of tin–substrate interactions and the low dimensionality of the film structure. In decomposing the Sn core-level spectra into metallic and oxi-

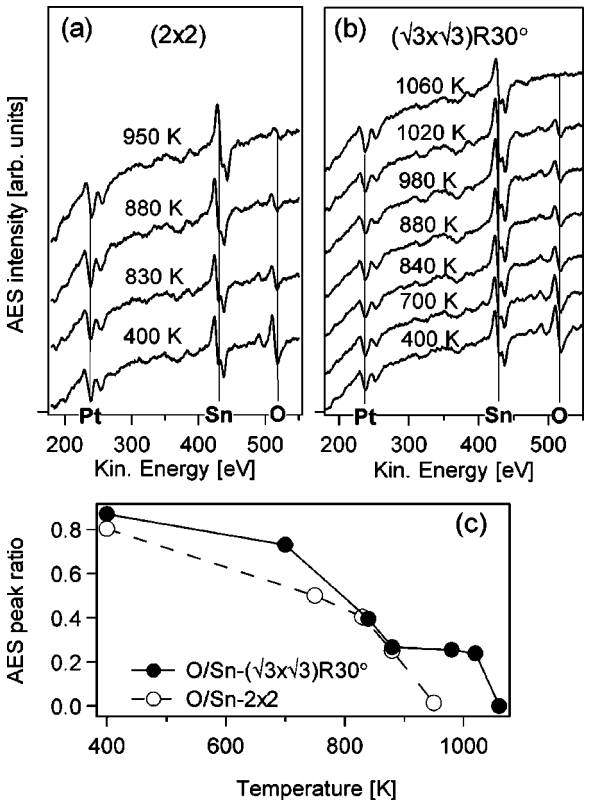

FIG. 1. AES spectra for successive annealing temperatures for the oxidized (a) (2×2)-Sn/Pt(111) and (b) $(\sqrt{3}\times\sqrt{3})R30°$-Sn/Pt(111) surface alloy. (c) Plot of AES peak ratios for the O (510 eV) and Sn (430 eV) peaks for alloys. The difference between the two alloys lies in the oxygen desorption above 800 K. While for the oxidized (2×2) surface alloy the oxygen diminishes rapidly above 800 K, the oxidized O/Sn ratio for the $(\sqrt{3}\times\sqrt{3})R30°$ alloy does not change significantly up to above 1000 K. Thus a stable oxide overlayer forms only for the oxidized $(\sqrt{3}\times\sqrt{3})R30°$ surface alloy in this temperature range.

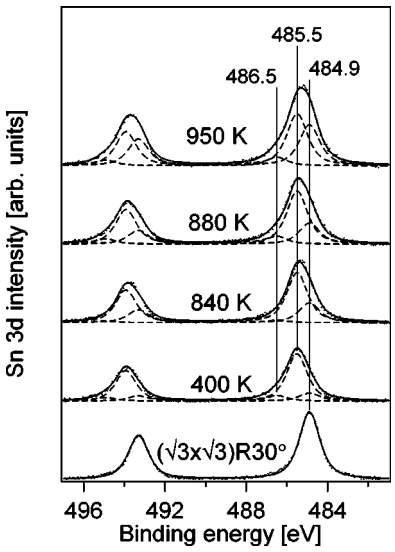

FIG. 2. Sn($3d$) XPS spectra for the metallic and oxidized $(\sqrt{3}\times\sqrt{3})R30°$ surface alloy at subsequently higher annealing temperatures. The peaks for the oxidized surface are deconvoluted into one metallic state and two oxidized states (dashed lines). A significant increase in the metallic Sn($3d$) component is apparent upon annealing to 950 K.

dized components, the line shape, full width at half maximum (FWHM), and spin-orbit splitting of the Sn($3d$) peaks of the clean $(\sqrt{3}\times\sqrt{3})R30°$ surface alloy were used to approximate all of the oxidized Sn components. The Sn peaks for the oxidized surfaces (Fig. 2) could be adequately fitted by a metallic component plus two oxidized Sn^{x+} components, associated with ''quasimetallic'' and Sn^{2+} species. The amount of Sn^{2+} component is much smaller than the quasimetallic component for all surfaces. Annealing the oxidized $(\sqrt{3}\times\sqrt{3})R30°$ surface alloy did not change significantly the intensity of the oxidized Sn components in the Sn($3d$) spectra. The increase in the Sn signal after annealing the sample to 840 K may be explained by the loss of surface oxygen, as was observed in TPD (Ref. 24) and AES (Fig. 1), because of a smaller attenuation of the XPS Sn signal by oxygen. However, some segregation of Sn to the near-surface region cannot be excluded. Between 840 and 880 K, only the intensity of the Sn^{2+} component increases but annealing to 950 K causes a significant increase in the overall Sn($3d$) signal because of an increase in the metallic Sn component. No oxygen desorbs between 840 and 1000 K, so Sn segregation from the bulk to the surface region must account for this increase. More tin must be deposited (1.0 ML) to prepare the alloy than is present in the topmost layer of the $(\sqrt{3}\times\sqrt{3})R30°$ surface alloy (0.33 ML), thus some subsurface tin is present and could account for the increase in the Sn($3d$) intensity.

C. LEED and STM

Combined LEED and STM studies of the oxidized Pt–Sn surface alloys reveal new information on surface structure. Dosing NO_2 on either surface alloy at 400 K results in a diffuse LEED image with no diffraction spots. Upon annealing the sample to 600 K, first-order Pt substrate spots appear on a diffuse background with no apparent additional ordering of the surface. A complex LEED pattern of diffuse spots for both alloy surfaces forms upon further annealing to 840 K, with the diffraction spots for the oxidized (2×2) alloy being fainter than those for the oxidized $(\sqrt{3}\times\sqrt{3})R30°$ alloy. STM images of the oxidized (2×2) alloy are presented in Fig. 3. The surface appears to be flat, with atomic steps similar to those observed on the clean alloy substrate. No islanding was observed, indicating that the SnO_x overlayer wets the Pt(111) substrate. In some cases, ''holes'' in the overlayer were observed. These holes were preferentially located in the center of terraces and have a depth measured at 0.15–0.20 nm. High resolution images showed some disordered structure but no atomic resolution images could be obtained. Even though further flash annealing to 880 K did not result in a clearly ordered LEED pattern, some locally ordered domains appear in STM images [Fig. 3(b)]. However, no atomic scale uniform surface structure could be found.

Annealing the $(\sqrt{3}\times\sqrt{3})R30°$ alloy to 860–880 K yields a distinct LEED pattern [Fig. 4(a) (inset)]. STM images of this structure reveal areas with bright rows separated by 1.2 nm

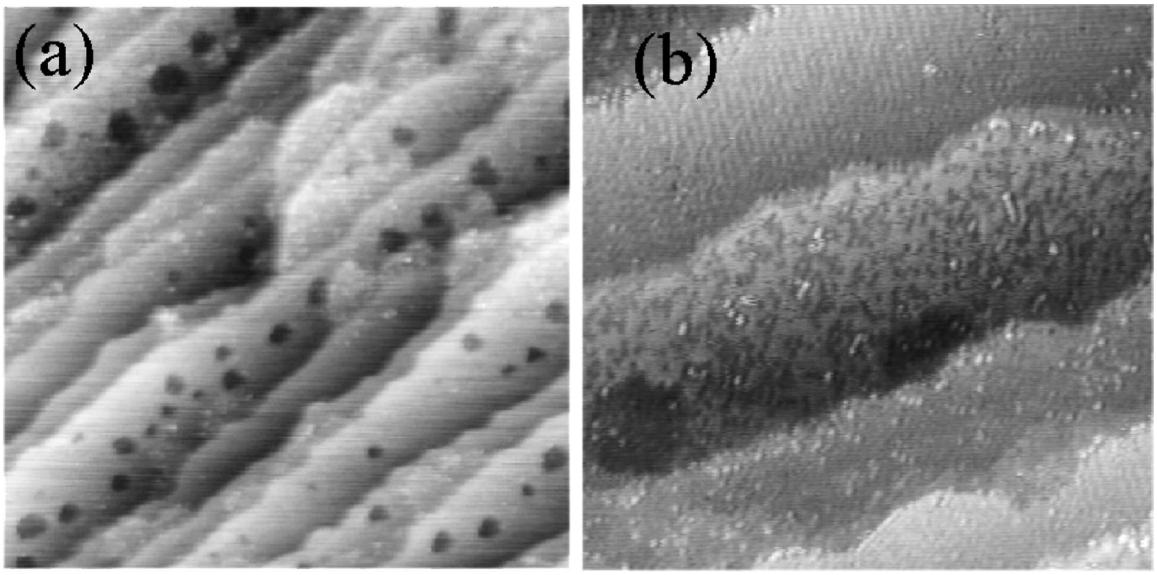

FIG. 3. (a) STM image of the oxidized (2×2)-Sn/Pt surface alloy after flash annealing to 830 K. Scan area: 115×115 nm^2. A SnO_x film wets the Pt(111) surface. Some terraces exhibit holes in the SnO_x film of ~0.2 nm depth. (b) STM image after further flash annealing to 880 K. Scan area: 40×40 nm^2. Domains of an ordered, periodic SnO_x film can be identified on some terraces (upper terrace). The terrace in the center of the STM image exhibits a disordered SnO_x film with irregularly distributed depressions.

[Fig. 4(a)]. These rows form a coincident lattice with a spacing five times the separation between Pt rows in the ⟨110⟩ direction of the Pt(111) substrate. Three domains, orientated 60° to each other, were observed. On top of the bright rows, protrusions were observed. Neighboring protrusions on adjacent rows preferentially form a 60° angle with respect to the row orientation. If this surface is repeatedly oxidized and annealed, an ordered SnO_x island structure is formed in a (5×5) superlattice [Fig. 4(b)]. This island superstructure has the same periodicity in one direction as the row structures of the surface depicted in Fig. 4(a), indicating that the LEED and STM features are a precursor state of a not fully oxidized island structure, and may represent strain relief patterns of a strained SnO_x adlayer. A detailed discussion of these features is beyond the scope of this article, but it can be found elsewhere.[39]

Further flash annealing of the $(\sqrt{3}\times\sqrt{3})R30°$ alloy to 900–1000 K (or annealing to 850 K for several minutes) results in the appearance of a (4×4) LEED pattern [Fig. 4(c) (inset)]. The appearance of this structure coincides with an increase of the metallic Sn component in XPS which results from tin segregation to the surface. Sn segregation is a thermally activated process, which is consistent with this transition taking considerably longer at lower temperatures. The STM images for this surface are shown in Fig. 4(c). The unit cell can be constructed from the protrusions in the images, with a separation of twice the Pt(111) lattice constant with every second protrusion missing in every second row. The missing protrusions define the (4×4) unit cell. The corrugation of these protrusions is 0.08–0.12 nm. The large corrugation of the protrusions implies that these are not just due to electronic effects, but also have a topographical origin. While the unit cell can be constructed from the STM images, it is apparent that many vacancies exist in the (4×4) superstructure [Fig. 4(c)].

Upon annealing of the surface to 1200 K, LEED and STM showed a well-ordered (2×2) lattice consistent with the formation of the Pt–Sn(111)-(2×2) surface alloy after complete decomposition of SnO_x species and desorption of all the remaining oxygen.

IV. DISCUSSION

Minimization of surface free energy is the driving force behind the formation of Sn/Pt surface alloys following Sn vapor deposition on Pt(111) and annealing.[40] Sn has the lower surface free energy compared to Pt, thus the system favors a high tin concentration at the surface. However, Pt–Sn bonds are quite favorable, thus the formation of a surface alloy is favored. If enough Sn is available, the stable $(\sqrt{3}\times\sqrt{3})R30°$ surface alloy structure is formed, which maximizes the number of Sn–Pt bonds and at the same time the amount of Sn in the surface layer. For insufficient Sn, a (2×2) surface alloy forms, which is also the bulk termination of the ordered Pt_3Sn alloy. Covering the Pt(111) surface with an oxide layer can also reduce the surface free energy of the system. Although a value for the surface energy of the SnO_x film cannot be given, it is apparent from our STM observations that the SnO_x film wets the surface and this indicates that the surface free energy of the oxide is less than that of the Pt(111) surface. From the XPS data of the oxidized $(\sqrt{3}\times\sqrt{3})R30°$ surface alloy we conclude that significant Sn segregation to the surface does not occur below 900 K for flash annealed samples. Thus, the interface between the SnO_x film and the substrate is likely to be a Pt(111) surface for samples flash annealed to temperatures below 900 K. A

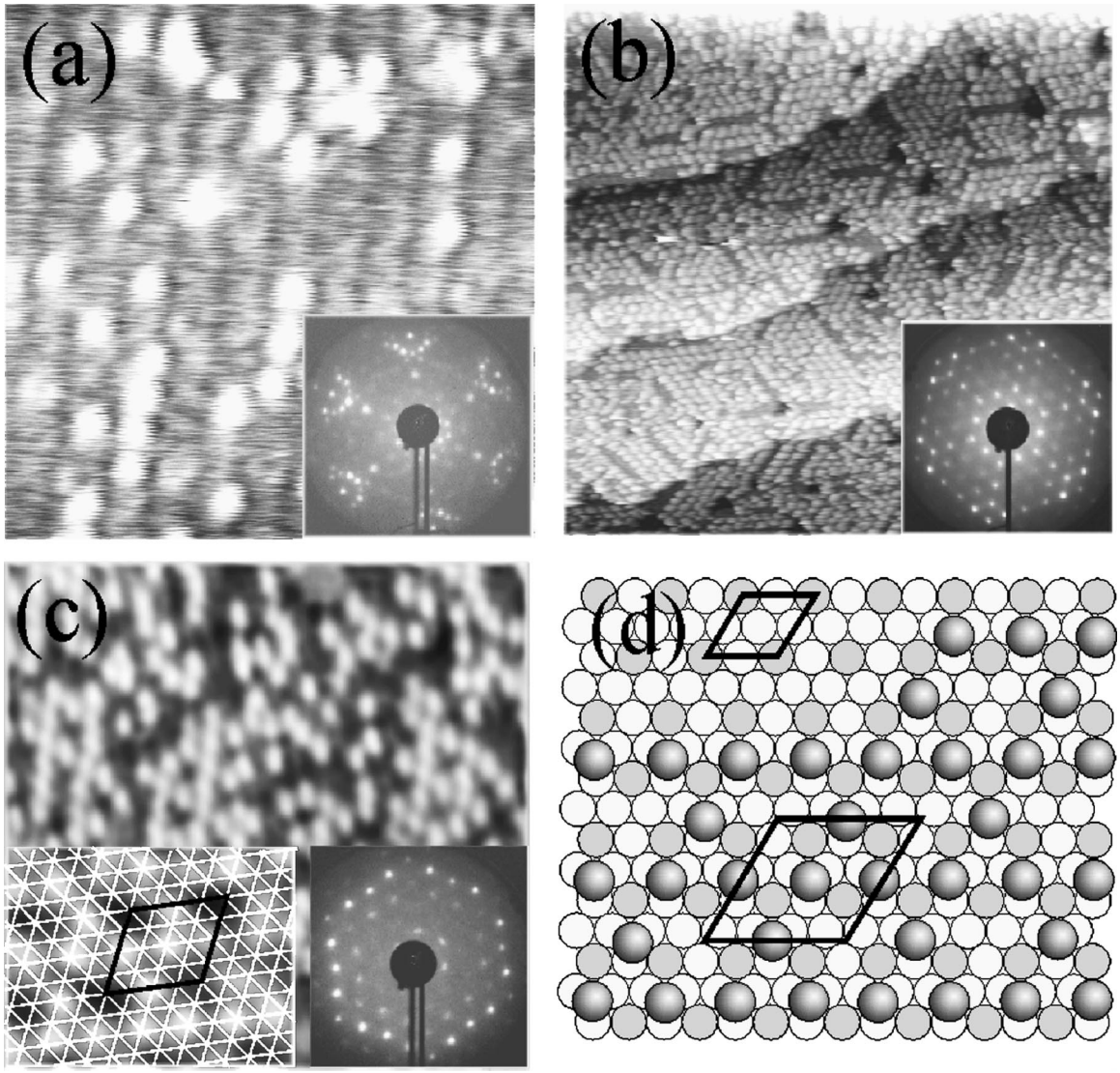

FIG. 4. STM images of an oxidized $(\sqrt{3}\times\sqrt{3})R30°$ surface alloy. (a) STM image (20 nm×20 nm) of the surface structure that forms if the oxidized surface is flash annealed to 840–890 K. The inset shows the LEED pattern ($E\sim70$ eV) from this surface. (b) STM image (62 nm×62 nm) of a (5×5) SnO_x island structure. This island structure forms after repeated reoxidation and annealing cycles of the surface shown in (a). The atomic steps in the image are similar to those observed on clean Pt(111). The inset shows the (5×5) LEED pattern ($E\sim70$ eV) from this surface. (c) STM image (12 nm×12 nm) of a surface showing a (4×4) LEED pattern. The inset on the left shows a STM image at higher resolution of a well-ordered surface area. The white lines indicate the Pt–substrate lattice; the (4×4) unit cell is also highlighted. The inset on the right shows the (4×4) LEED pattern ($E\sim70$ eV) from this surface. (d) Proposed model for the (4×4) superstructure. In this model the (4×4) structure is formed by Sn_xO_y species (shaded circles) sitting on top of a (2×2)-Sn/Pt(111) alloy. Both unit cells for the (2×2) and (4×4) structure are indicated. It is proposed that the Sn_xO_y species preferentially adsorb on the Pt ensembles of the (2×2) Sn/Pt(111) surface alloy, thus lowering the surface energy and allowing Sn–Pt bonds to form.

Pt(111) interface is also likely to exist for oxidized (2×2) surface alloys since even less tin is present at this surface. However, the fact that Sn eventually segregates to the interfacial region at elevated temperatures indicates that formation of an interface Sn/Pt alloy is energetically favored over a Pt(111) interface even for the oxide covered surface.

The previously observed distinct difference in the oxidation of the two Sn/Pt(111) surface alloys has been confirmed in this study. While the oxidized $(\sqrt{3}\times\sqrt{3})R30°$ surface alloy forms a tin oxide overlayer that orders in a (4×4) structure upon flash annealing to above 900 K, the oxidized (2×2) surface alloy never exhibits an ordered structure over an extended surface area and readily decomposes in a wide temperature range between 840 and 1000 K. The experiments presented here were designed to test proposed explanations for the differences in behavior between the two oxidized surface alloys. Prior to this structural study the formation of SnO_x islands with a wide island size distribution was discussed. This was suggested to explain the observed TPD spectra for the oxidized (2×2) surface alloy by assuming island size-dependent SnO_x decomposition temperatures. Based on our results such speculation can now be discarded. Even though the oxidized (2×2) surface alloy exhibits holes in the oxide adlayer after annealing to 840 K (above the desorption temperature of oxygen chemisorbed on Pt sites), the film clearly wets the surface and does not form

three-dimensional (3D) islands. The presence of holes, on the other hand, implies that not enough tin was initially available to form a uniform overlayer. We propose that the incomplete covering of the Pt(111) surface after oxidation of the (2×2) surface alloy explains the decomposition of this film over a wide temperature range. Clean Pt(111) ''patches'' possess a high surface energy. The reduction of this surface energy by alloying with tin may provide the necessary activation energy to break Sn–O bonds at lower temperatures. Kinetic limitation of this process, in particular tin diffusion in the surface layer may explain the wide temperature range over which the oxide layer decomposes. For the oxidized $(\sqrt{3}\times\sqrt{3})R30°$ surface alloy, a uniform surface layer was observed that formed a pseudoordered intermediate structure [Fig. 4(a)]. This structure was associated with a strain relief pattern, rather than with atomic ordering.[35] Such an ordered strain relief pattern also indicates a uniform layer. Sn–O bonds in a complete layer may be more difficult to break and thus form a more thermally stable film.

Sn segregation from the bulk to the SnO_x–Pt interface and the proposed formation of a (2×2) interface alloy change the surface considerably and a (4×4) ordered structure is observed. The unit cell of the (4×4) structure is easily determined from LEED and STM. Because the protrusions form a coincident lattice with the Pt(111) and with the (2×2) Sn/Pt(111) surface alloy (as is usually observed for the adsorption of molecules on surfaces), it is tempting to propose a model which identifies the protrusions as Sn_xO_y ''molecules'' populating energetically favorable substrate sites. The number of oxidized Sn atoms on the surface may be estimated by assuming that all the Sn from a $(\sqrt{3}\times\sqrt{3})R30°$ surface alloy is oxidized after the first oxidation step. This amounts to 0.33 ML of Sn on the surface. The number of protrusions in the (4×4) unit cell indicates a maximum Sn_xO_y coverage of 19%. This implies two Sn atoms per protrusion in the (4×4) structure. The large number of defects in the (4×4) structure and disordered areas on the surface can easily account for the differences between 0.33 and $2\times0.19=0.38$. Previous TPD studies estimated the oxygen coverage for the (4×4) structure at 0.1–0.15 ML.[24] This implies that the stoichiometry of the tin-oxide molecules is closer to Sn_2O than to SnO. This is consistent with our expectation of two Sn atoms per protrusion in the (4×4) structure.

As mentioned above, the formation of the Sn/Pt surface alloy results from minimizing the surface free energy and maximizing the number of Sn–Pt bonds. Thus we speculate that similar behavior exists for the oxidic Sn_2O particles and consequently they may preferentially populate the Pt sites on a (2×2)-Sn/Pt(111) surface alloy substrate. In such a scenario most of the Pt at the surface is covered and Sn–Pt bonds between the tin-oxide species and the substrate can be formed. Although, no direct evidence for the adsorption sites of the Sn_2O particles is available, we propose a model based on the above considerations [Fig. 4(d)].

[1] R. D. Cortright and J. A. Dumesic, J. Catal. **157**, 576 (1995).
[2] G. B. Hoflund, D. A. Ashbury, and R. E. Gilbert, Thin Solid Films **129**, 139 (1985).
[3] F. M. Dautzenberg, J. N. Helle, P. Biloen, and W. M. H. Sachtler, J. Catal. **63**, 119 (1980).
[4] J. Voelter, G. Lietz, M. Uhlemann, and M. Hermann, J. Catal. **68**, 42 (1981).
[5] K. Grass and H. G. Lintz, *4th International Conference on Spillover, Dalian, China, 1997*, edited by C. Li and Q. Xin (Elsevier, Amsterdam, 1997), p. 135.
[6] R. Bouwman, L. H. Toneman, and A. A. Holsher, Surf. Sci. **35**, 8 (1973).
[7] R. Bouwman and P. Biloen, Anal. Chem. **46**, 136 (1974).
[8] R. Bouwman and P. Biloen, Surf. Sci. **41**, 348 (1974).
[9] P. Biloen, R. Bouwman, R. A. van Santen, and H. H. Brongerman, Appl. Surf. Sci. **2**, 532 (1979).
[10] G. B. Hoflund, D. A. Asbury, P. Kirszensztejn, and H. A. Laitinen, Surf. Interface Anal. **9**, 169 (1986).
[11] S. D. Gardner, G. B. Hoflund, M. R. Davidson, and D. R. Schryer, J. Catal. **115**, 132 (1989).
[12] D. A. Asbury and G. B. Hoflund, Surf. Sci. **199**, 552 (1988).
[13] S. D. Gardener, G. B. Hoflund, and D. R. Schryer, J. Catal. **119**, 179 (1989).
[14] W. Unger and D. Marton, Surf. Sci. **218**, L467 (1989).
[15] D. F. Cox, G. B. Hoflund, and H. A. Laitinen, Langmuir **1**, 269 (1985).
[16] G. B. Hoflund, D. A. Asbury, and R. E. Gilbert, Thin Solid Films **129**, 139 (1985).
[17] H. Lieske and J. Voelter, J. Catal. **90**, 96 (1984).
[18] R. Bacaud, P. Bussiere, and F. Figueras, J. Catal. **69**, 399 (1981).
[19] G. B. Hoflund, D. A. Asbury, P. Kirszensztejn, and H. A. Laitinen, Surf. Sci. **161**, L583 (1985).
[20] C. Gallis, B. Legrand, and G. Treglia, Surf. Sci. **377–379**, 1033 (1997).
[21] M. T. Paffett and R. G. Windham, Surf. Sci. **208**, 34 (1989).
[22] S. H. Overbury, D. R. Mullin, and B. E. Koel, Surf. Sci. **254**, 45 (1989).
[23] A. Atrei, U. Bardi, J. X. Wu, E. Zanazzi, and G. Rovida, Surf. Sci. **290**, 286 (1993).
[24] N. A. Saliba, Y. L. Tsai, and B. E. Koel, J. Phys. Chem. B **103**, 1532 (1999).
[25] N. A. Saliba, Ph.D. thesis, University of Southern California, Los Angeles (1999).
[26] K. D. Schierbaum, Surf. Sci. **399**, 29 (1998).
[27] K. Wilson, A. F. Lee, C. Hardacre, and R. M. Lambert, J. Phys. Chem. B **102**, 1736 (1998).
[28] P. S. Robbert, H. Geisler, C. A. Ventrice, Jr., J. van Ek, S. Chaturvedi, J. A. Rodriguez, M. Kuhn, and U. Diebold, J. Vac. Sci. Technol. A **16**, 990 (1998).
[29] M. Ritter, W. Ranke, and W. Weiss, Phys. Rev. B **57**, 7240 (1998).
[30] W. Ranke, M. Ritter, and W. Weiss, Phys. Rev. B **60**, 1527 (1999).
[31] Y. Zhang and A. J. Slavin, Phys. Rev. B **49**, 2005 (1994).
[32] A. F. Lee and R. M. Lambert, Phys. Rev. B **58**, 4156 (1998).
[33] A. F. Lee, C. J. Baddeley, M. S. Tikhov, and R. M. Lambert, Surf. Sci. **373**, 195 (1997).
[34] T. Fujii, D. Alders, F. C. Voogt, T. Hibma, B. T. Thole, and G. A. Sawatzky, Surf. Sci. **366**, 579 (1996).
[35] T. Fujii, F. M. F. de Groot, G. A. Sawatzky, F. C. Voogt, T. Hibma, and K. Okada, Phys. Rev. B **59**, 3195 (1999).
[36] F. C. Voogt, T. Hibma, G. L. Zhang, M. Hoefman, and L. Nielsen, Surf. Sci. **331–333**, 1508 (1995).
[37] F. C. Voogt, T. Fujii, P. J. M. Smulders, L. Nielsen, M. A. James, and T. Hibma, Phys. Rev. B **60**, 11193 (1999).
[38] J. M. Themlin, M. Chtaib, L. Henrard, P. Lambin, J. Darville, and J. M. Gilles, Phys. Rev. B **46**, 2460 (1992).
[39] M. Batzill, D. E. Beck, and B. E. Koel, Appl. Phys. Lett. (submitted).
[40] U. Bardi, Rep. Prog. Phys. **57**, 939 (1994).